ACS OMEGA

http://pubs.acs.org/journal/acsodf

Article

Utilization of Guanidine-Based Ancillary Ligands in Arene−Ruthenium Complexes for Selective Cytotoxicity

Jit Karmakar, Promita Nandy, Saurabh Das, Debalina Bhattacharya, Parimal Karmakar, and Samaresh Bhattacharya*

Cite This: *ACS Omega* 2021, 6, 8226−8238

Read Online

ACCESS | Metrics & More | Article Recommendations | Supporting Information

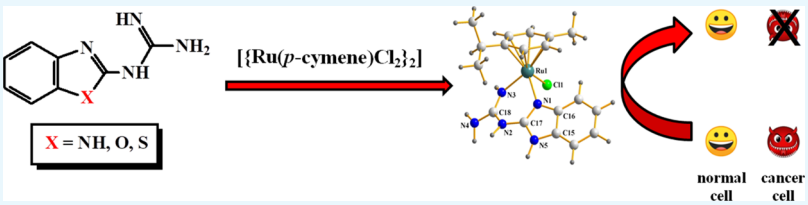

ABSTRACT: A family of three water-soluble half-sandwich arene−ruthenium complexes, depicted as C_1−C_3, having the general formula [Ru(*p*-cymene)(L)Cl]Cl has been synthesized, where L represents (1*H*-benzo[*d*]imidazol-2-yl)guanidine (L_1) or (benzo[*d*]oxazol-2-yl)guanidine (L_2) or (benzo[*d*]thiazol-2-yl)guanidine (L_3). The crystal structure of complex C_3 has been determined. The complexes show several absorption bands in the visible and ultraviolet regions, and they also show prominent emission in the visible region while excited near 400 nm. Studies on the interaction of ligands L_1−L_3 and complexes C_1−C_3 with calf thymus DNA reveal that the complexes are better DNA binders than the ligands, which is attributable to the imposed planarity of the ruthenium-bound guanidine-based ligand, enabling it to serve as a better intercalator. Molecular docking studies show that the complexes effectively bind with DNA through electrostatic and H-bonding interactions and partial intercalation of the guanidine-based ligands. Cytotoxicity studies carried out on two carcinoma cell lines (PC3 and A549) and on two non-cancer cell lines (BPH1 and WI-38) show a marked improvement in antitumor activity owing to complex formation, which is attributed to improvement in cellular uptake on complex formation. The C_1 complex is found to exhibit the most prominent activity against the PC3 cell line. Inclusion of the guanidine-based ligands in the half-sandwich ruthenium−arene complexes is found to be effective for displaying selective cytotoxicity to cancer cells and also for convenient tracing of the complexes in cells due to their prominent emissive nature.

1. INTRODUCTION

Development of a new series of therapeutic agents and modification of any existing series are an essential and challenging aspect of research related to the treatment of cancer. Platinum metal-based species, especially coordination and organometallic complexes, are widely employed as chemotherapeutics in combating this dreadful disease.[1] However, relatively low selectivity and adverse side effects of majority of these species have led to new initiatives toward development of better chemotherapeutic agents, particularly of new platinum metal-based anticancer complexes with minimal side effects and high selectivity and cytotoxicity toward cancer cells.

Among the platinum metal-based species, ruthenium compounds have found a very special position owing to their prominent anticancer activities.[2] Ruthenium-based molecular species are found to be promising candidates for the development of novel anticancer agents, primarily as they can bind DNA in several possible modes, a property usually not found in platinum-based species. Hence, the ruthenium-based species also have the potential to treat platinum-resistant cancers. Among the different oxidation states of ruthenium, the +2 state is most preferred for antitumor activity due to stability of the ruthenium(II) complexes in vitro. Proper choice of a ligand scaffold is crucial for inducing the desired DNA binding and antitumor activity in the ruthenium(II) complexes. In this context, half-sandwich ruthenium−arene complexes are particularly noteworthy.[3,4] The presence of the planar arene moiety primarily blocks one face of the complex and thus directs most of the reactivity toward the other side. Besides, *para*-cymene, a heavily used arene moiety, is known to cause distortion in DNA conformation that eventually leads to DNA damage.[5] In half-sandwich ruthenium−arene complexes, there is ample scope of varying the ligand/ligand combination to occupy the remaining three coordination sites on the metal center. In the present work, where our main objective was to develop a new family of half-sandwich ruthenium−arene

Received: December 24, 2020
Accepted: March 11, 2021
Published: March 19, 2021

complexes for efficient DNA binding and anticancer activity, a group of three guanidine-based compounds was selected (Chart 1) as ancillary ligands. These ligands have several

Chart 1

X	L
NH	L_1
O	L_2
S	L_3

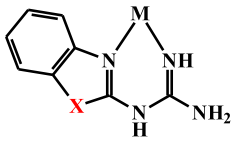

I

important features, which are favorable for developing efficient DNA binding and anticancer agents. They have multiple N−H bonds, which are expected to favor solubility in water and binding with pyrimidine or purine bases via H-bonding and thus mislead the transcription process, resulting in DNA damage. In addition, the near-planar geometry of these ligands may enable them to function as intercalating moieties in the derived ruthenium complexes.[3c,h,6] The skeleton of the selected ligands has close resemblance with that of 4′,6-diamidino-2-phenylindole (DAPI), a conjugated system that is known to efficiently stain DNA present in a cell,[7] which further encouraged us to use this group of ligands, with the hope that the mixed-ligand half-sandwich complexes derived from them may exhibit luminescence property and thus, they will be useful for measuring the capacity for cellular uptake and track a molecule within a cell. Among the three chosen ligands, synthesis of L_1 and L_2 and complexes of L_1 with few metals are known in the literature,[8,9] while L_3 is, to the best of our knowledge, new and coordination chemistry of L_2 and L_3 appears to remain unexplored. The L_1 ligand is known to coordinate metal centers as a bidentate N,N-donor, forming a stable six-membered chelate ring (**I**, X = NH),[9] and the L_2 and L_3 ligands are likely to display a similar mode of binding (**I**, X = O and S). As a source of ruthenium(II) and the arene moiety the dimeric $[\{Ru(p\text{-cymene})Cl_2\}_2]$ compound was utilized. Reaction of the selected guanidine-based ligands (L_1−L_3) with $[\{Ru(p\text{-cymene})Cl_2\}_2]$ indeed afforded half-sandwich ruthenium−arene complexes containing the ligands L_1−L_3. Herein, we describe the formation and characterization of these complexes, their DNA binding properties, and their cytotoxicity toward selected cancer cell lines.

2. EXPERIMENTAL SECTION

2.1. Materials. Ruthenium trichloride was purchased from Arora Matthey, Kolkata, India. α-Phellandrene, $[Ru(bpy)_3](ClO_4)_2$, and dicyandiamide were purchased from Sigma-Aldrich, USA. *o*-Phenylenediamine, 2-aminophenol, and 2-aminothiophenol were procured from Spectrochem, India. The guanidine-based ligands (L_1−L_3) were synthesized by reaction between *o*-phenylenediamine (or 2-aminophenol or 2-aminothiophenol) and dicyandiamide following a reported protocol.[8] $[\{Ru(p\text{-cymene})Cl_2\}_2]$ was synthesized by following a published procedure.[10] All other chemicals and solvents were reagent-grade commercial materials and were used as received.

2.2. Physical Measurements. Microanalyses (C, H, and N) were performed on a Heraeus Carlo Erba 1108 elemental analyzer. Magnetic susceptibilities were measured using a Sherwood MK-1 balance. NMR spectra were recorded in $CDCl_3$ solution on Bruker Avance DPX 300 and 400 NMR spectrometers. IR spectra were obtained on a PerkinElmer Spectrum Two spectrometer with samples prepared as KBr pellets. Mass spectra were recorded with a Micromass LCT electrospray (Qtof Micro YA263) mass spectrometer. Electronic spectra were recorded on a PerkinElmer LAMBDA 25 spectrophotometer. Steady-state emission spectra were collected on a PerkinElmer LS 55 fluorescence spectrometer, and the quantum yields were determined by a relative method using $[Ru(bpy)_3]^{2+}$ as the standard. Solution electrical conductivities were measured using an Elico CM 180 conductivity meter with a solute concentration of *ca.* 10^{-3} M. Geometry optimization by the density functional theory (DFT) method and electronic spectral analysis by TDDFT calculation were performed using the Gaussian 09 (B3LYP/SDD-6-31G) package.[11]

2.3. X-ray Crystallography. Single crystals of $[Ru(p\text{-cymene})(L_3)Cl]Cl$ (C_3) were grown by diffusion of diethyl ether vapor into a solution of the complex in acetonitrile. Selected crystal data and data collection parameters are given in Table 1. Data were collected on a Bruker SMART CCD

Table 1. Crystal Data and Details of the Structure Determination for Complex C_3

empirical formula	$C_{18}H_{24}Cl_2N_4ORuS$
formula mass	516.45
crystal system	orthorhombic
space group	$P2_12_12_1$
a (Å)	7.5864(4)
b (Å)	12.9878(7)
c (Å)	21.6163(12)
V (Å^3)	2129.9(2)
Z	4
D_{calcd} (g/cm^3)	1.611
F(000)	1048
crystal size (mm)	0.16 × 0.18 × 0.24
T (K)	296
μ (mm^{-1})	1.101
R_1[a]	0.0452
wR_2[b]	0.1175
GOF[c]	1.03

[a]$R_1 = \Sigma||F_o| - |F_c||/\Sigma|F_o|$. [b]$wR_2 = [\Sigma[w(F_o^2 - F_c^2)^2]/\Sigma[w(F_o^2)^2]]^{1/2}$. [c]$GOF = [\Sigma[w(F_o^2 - F_c^2)^2]/(M - N)]^{1/2}$, where *M* is the number of reflections and *N* is the number of parameters refined.

diffractometer using graphite monochromated Mo Kα radiation (λ = 0.71073 Å) at 296 K. X-ray structure solution and refinement were done using the SHELX-97 package.[12] H atoms were added at calculated positions.

2.4. Synthesis of Complexes. The $[Ru(p\text{-cymene})(L)Cl]Cl$ complexes (C_1−C_3) were synthesized by following a general procedure as described below.

The guanidine-based ligand (L_1−L_3) (0.2 mmol) was dissolved in hot methanol (50 mL). To it was added a solution of $[\{Ru(p\text{-cymene})Cl_2\}_2]$ (50 mg, 0.08 mmol) in dichloromethane (10 mL). The resulting solution was heated at reflux for 4 h to generate a yellowish-orange solution. The solvent was evaporated to almost one-fourth of its initial volume, diethyl ether (50 mL) was added to it, and the mixture was kept in a freezer for 12 h. Orange crystalline solid was

https://doi.org/10.1021/acsomega.0c06265
ACS Omega 2021, 6, 8226−8238

separated, which was collected by filtration, washed with dichloromethane followed with diethyl ether, and dried in air.

2.4.1. [Ru(p-cymene)(L_1)Cl]Cl (C_1). Yield: 79%. Anal. Calcd for $C_{18}H_{23}N_5Cl_2Ru$: C, 44.90; H, 4.78; N, 14.55. Found: C, 45.02; H, 4.68; N, 14.42%. MS-ES$^+$ in CH_3OH (m/z): 410.1216 $[M - HCl{-}Cl^-]^+$. IR data/cm^{-1}: 3367, 2969, 1673, 1611, 1581, 1462, 1268. ^{1}H NMR (DMSO-d_6, 500 MHz): δ (ppm) 7.43 (br s, 1H, NH), 7.28 (m, 2H, ArH), 7.09 (m, 2H, ArH), 6.03 (d, 2H, ArH, $^3J_{HH}$ = 5.6 Hz), 5.87 (d, 2H, ArH, $^3J_{HH}$ = 5.5 Hz), 3.43 (m, 1H, CH), 2.49 (s, 3H, CH_3), 1.01 (m, 6H, $2CH_3$). ^{13}C NMR (DMSO-d_6, 400 MHz): δ (ppm) 158.6, 152.3, 129.2, 126.4, 122.0, 112.4, 111.5, 30.5, 24.3. Molar conductivity in methanol at 298 K [Λ_M/S m^2 M^{-1}]: 83.

2.4.2. [Ru(p-cymene)(L_2)Cl]Cl (C_2). Yield: 74%. Anal. Calcd for $C_{18}H_{22}N_4O_1Cl_2Ru$: C, 44.81; H, 4.56; N, 11.61. Found: C, 44.50; H, 4.41; N, 11.91%. MS-ES$^+$ in CH_3OH (m/z): 411.1928 $[M - HCl{-}Cl^-]^+$. IR data/cm^{-1}: 3392, 1690, 1620, 1562, 1457, 1324, 1243. ^{1}H NMR (DMSO-d_6, 500 MHz): δ (ppm) 7.91 (br s, NH), 7.50 (d, 1H, ArH, $^3J_{HH}$ = 8.0 Hz), 7.48 (d, 1H, ArH, $^3J_{HH}$ = 8.0 Hz), 7.27 (m, 1H, ArH), 7.21 (m, 1H, ArH), 5.77 (d, 1H, ArH, $^3J_{HH}$ = 6.0 Hz), 5.72 (d, 1H, ArH, $^3J_{HH}$ = 5.5 Hz), 2.80 (m, 1H, CH), 2.50 (s, 3H, CH_3), 1.17 (m, 6H, $2CH_3$). ^{13}C NMR (DMSO-d_6, 400 MHz): δ (ppm) 158.1, 154.5, 135.5, 122.2, 116.0, 110.2, 106.3, 43.4, 35.6. Molar conductivity in methanol at 298 K [Λ_M/S m^2 M^{-1}]: 81.

2.4.3. [Ru(p-cymene)(L_3)Cl]Cl (C_3). Yield: 81%. Anal. Calcd for $C_{18}H_{22}N_4S_1Cl_2Ru$: C, 43.37; H, 4.41; N, 11.24. Found: C, 43.20; H, 4.43; N, 11.40%. MS-ES$^+$ in CH_3OH (m/z): 427.0103 $[M - HCl{-}Cl^-]^+$. IR data/cm^{-1}: 3408, 3246, 2964, 2817, 1680, 1613, 1598, 1520, 1445, 1390, 1284, 1254, 1230. ^{1}H NMR (DMSO-d_6, 400 MHz): δ (ppm) 7.25 (s, NH), 6.96 (d, 2H, ArH, $^3J_{HH}$ = 8.5 Hz), 6.73 (d, 2H, ArH, $^3J_{HH}$ = 8.5 Hz), 5.20 (br m, 2H, ArH), 4.96 (br m, 2H, ArH), 2.99 (m, 1H, CH), 1.59 (s, 3H, CH_3), 1.40 (m, 6H, $2CH_3$). ^{13}C NMR (DMSO-d_6, 500 MHz): δ (ppm) 160.1, 157.5, 152.0, 125.6, 120.0, 102.5, 30.7, 22.6. Molar conductivity in methanol at 298 K [Λ_M/S m^2 M^{-1}]: 85.

2.5. Biological Studies. *2.5.1. Interaction with CT-DNA.* Phosphate buffer was prepared using NaH_2PO_4 and Na_2HPO_4 using triple-distilled water. Sodium nitrate (AR) was used to maintain the ionic strength of the medium. Calf thymus DNA, purchased from Sisco Research Laboratories, India, was dissolved in triple-distilled water containing 120 mM NaCl, 35 mM KCl, and 5 mM $CaCl_2$. Absorbance was recorded at 260 and 280 nm; A_{260}/A_{280} was determined. The ratio being between 1.8 and 1.9 suggests that the DNA was sufficiently free from protein. It was characterized by measuring its CD spectrum at 260 nm using a CD spectropolarimeter (J815, JASCO). Concentration was determined in terms of nucleotide, considering the molar extinction coefficient at 260 nm to be 6600 M^{-1} cm^{-1}.

50 μM $\mathbf{L_1}$ (ligand) and 50 μM $\mathbf{C_1}$ (complex) were titrated separately with calf thymus DNA at constant pH and ionic strength of the medium. For the interaction of $\mathbf{L_1}$ followed by fluorescence spectroscopy, excitation was done at 295 nm and emission was recorded at 331 nm. For the complex, the excitation was done at 425 nm and emission was recorded at 496 nm. Ionic strength was maintained using NaCl and $NaNO_3$. The interaction of the compounds with DNA during titration led to a decrease in fluorescence in the case of the ligand and to an increase in fluorescence for the complex at the respective wavelengths where they were followed. The interaction of compounds with DNA could be realized with eq 1.[13−18]

$$L + DNA \rightleftharpoons L - DNA \qquad K_d = \frac{[L][DNA]}{[L - DNA]} \tag{1}$$

L represents compounds and K_d is the dissociation constant for the interaction whose reciprocal provides the apparent binding constant (K_{app}). Equation 2 is obtained from eq 1 where the reciprocal of the change in absorbance was plotted against the reciprocal of $(C_D - C_0)$.[13−18] C_D refers to concentration of calf thymus DNA and C_0 refers to concentration of compounds. Using eq 2, ΔF_{max} could be determined along with K_{app} ($1/K_d$) from the intercept and slope.[13−18]

$$\frac{1}{\Delta F} = \frac{1}{\Delta F_{max}} + \frac{K_d}{\Delta F_{max}(C_D - C_L)} \tag{2}$$

ΔF represents the change in fluorescence of the compounds interacting with the calf thymus DNA during titration, while ΔF_{max} indicates the maximum possible change in fluorescence.

$$K_d = \frac{\left[C_L - \left(\frac{\Delta F}{\Delta F_{max}}\right)C_L\right]\left[C_D - \left(\frac{\Delta F}{\Delta F_{max}}\right)C_L\right]}{\left(\frac{\Delta F}{\Delta F_{max}}\right)C_L} \tag{3}$$

$$C_L\left(\frac{\Delta F}{\Delta F_{max}}\right)^2 - (C_L + C_D + K_d)\left(\frac{\Delta F}{\Delta F_{max}}\right) + C_D = 0 \tag{4}$$

$\Delta F/\Delta F_{max}$ was plotted against C_D. Equations 3 and 4 were used to fit the data to a non-linear square fit that provides another set of values for the apparent binding constant.[13−18] Titrations were also analyzed using a modified form of the Scatchard equation [eq 5].[19] The overall binding constant (K') and site size (n) were determined.

$$\frac{r}{C_f} = K'(n - r) \tag{5}$$

r denotes the ratio of the concentration of the compound bound to DNA to the total concentration of DNA present in the reaction mixture at any point of the titration (C_b/C_D); C_b is the concentration of the bound compound, while C_f is that of the free compound. "n" provides binding stoichiometry in terms of the bound compound per nucleotide, while "n_b" being the reciprocal of "n" denotes binding site size in terms of the number of nucleotides bound to a compound. "n_b" was obtained by plotting $\Delta F/\Delta F_{max}$ against C_D/[compound]. K' may also be obtained by multiplying K_{app} with "n_b" and is compared with values obtained from a modified form of the Scatchard equation.

2.5.2. Molecular Docking Studies. Molecular docking studies on complexes $\mathbf{C1}-\mathbf{C_3}$ were performed using HEX 6.3 software to identify possible binding sites in biomolecules. The three guanidine-based ligands ($\mathbf{L_1}-\mathbf{L_3}$) were also docked using AutoDockTools 1.5.6 software. The coordinates of each ruthenium complex were taken from its optimized structure as a .mol file and converted to a .pdb format using PyMOL 2.4 software. The crystal structure of B-DNA (PDB ID: 1BNA) was retrieved from the Protein Data Bank (http://www.rcsb.org./pdb). Visualization of the docked systems was performed using BIOVIA Discovery Studio Visualizer (DSV) 2020 software. Default parameters were used for docking calculations with the correlation type shape only, FFT mode at the

https://doi.org/10.1021/acsomega.0c06265
ACS Omega 2021, 6, 8226−8238

3D level, and grid dimension of 0.6 with receptor range 180 and ligand range 180 with twist range 360 and distance range 40.

2.5.3. Cell Culture. PC3, BPH1, A549, and WI-38 lung fibroblast cells were cultured in RPMI or DMEM medium (GIBCO, Invitrogen, Carlsbad, CA, US) supplemented with 10% fetal bovine serum (GIBCO), 100 IU/mL penicillin, and 100 μg/mL streptomycin at 37 °C in a humidified atmosphere containing 5% CO_2 (Heraeus, Thermo Scientific, MA, USA). All cell lines were procured from the National Centre for Cell Science in Pune, India. Cells were seeded in 96 well plates for 24 h prior to treatment with compounds.

2.5.4. MTT Assay. The antiproliferative effect of three complexes and the guanidine-based ligands on four cell lines, PC3, BPH1, A549, and WI-38 was determined by the MTT assay. Cells were seeded at a density of 1×10^4 cells per well in a 24-well plate. Next, the cells were exposed to the complex and its ligand at different concentrations for another 24 h. After incubation, cells were washed with 1× PBS twice. Thereafter, they were treated with 0.5 mg mL^{-1} MTT solution (SRL) and incubated for 3−4 h at 37 °C until an insoluble purple-colored formazan product developed. The resulting product was dissolved in MTT extraction buffer and the OD was measured at 570 nm using a microplate reader (Epoch). The percentage survival was calculated considering the untreated cells as 100%.

2.5.5. Single-Cell Gel Electrophoresis/Comet Assay. A comet assay was performed after treating the cells (PC3 and BPH1) with complex $\mathbf{C_1}$ for 24 h at the lower (20 μM) and higher (80 μM) concentrations of the IC_{50} dose of 39.5 μM for PC3. Briefly, 1×10^5 cells mL^{-1} were mixed with 0.7% LMPA and embedded onto frosted slides. The slides were then dipped in a lysis solution [2.5 M NaCl, 100 mM EDTA, 10 mM Tris−HCl (pH 10)] that contains freshly added 1% Triton-X 100 and 10% DMSO and incubated for 1 h at 4 °C and placed into a horizontal electrophoresis tank filled with freshly prepared buffer (1 mM EDTA, 300 mM NaOH). Next, electrophoresis was performed for 20 min at a fixed voltage of 25 V and 300 mA. After that, slides were washed with a neutralization buffer (0.4 M Tris−HCl, pH 7.5) followed by staining with 20 mg mL^{-1} ethidium bromide (SRL, India) for 15 min. The slides were then washed three times with 1× PBS and observed under a fluorescence microscope (model: Leica, Germany). Around 50 comets per slide were counted for both the cell lines. An extension of each comet was analyzed using a computerized image analysis system (Kometsoftware 5.5) that gave % of tail DNA.[20]

2.5.6. DAPI Staining. After exposure with complex $\mathbf{C_1}$ at lower and higher concentrations of the IC_{50} dose of PC3 (39.5 μM) for 24 h, both the cells (PC3 and BPH1) were washed several times with 1× PBS and stained with 0.2 mg mL^{-1} DAPI in Vecta shield (Vector Laboratories Inc.). The percentage of cells with ruptured and decondensed nuclei was counted under a fluorescence microscope (Leica) and photographs were taken at 40× magnification.

2.5.7. Measurement of Intracellular Reactive Oxygen Species. The production of intracellular reactive oxygen species (ROS) was estimated using a fluorescent dye, DCFDA. Approximately, 3×10^5 cells per well were seeded in 35 mm plates, and after 24 h of seeding, cells were incubated with 20 μM DCFDA (Sigma) dye for 1 h at 37 °C under dark conditions followed by the treatment of complex $\mathbf{C_1}$ for 24 h, at the lower (20 μM) and higher (80 μM) concentrations of the IC_{50} doses of PC3 (39.5 μM). Cells without the complex were used as control. Fluorescence intensity was measured in a fluorescence spectrophotometer (model Hitachi, USA) at excitation and emission wavelengths of 504 and 529 nm, respectively. To nullify the autofluorescence of the complex which may interfere with the DCFDA dye, a set of experiments without cells were performed simultaneously.

2.5.8. Cellular Imaging Study. Both the cell lines PC3 and BPH1 were seeded in a cover slip for overnight. Next day, cells were incubated with 3 mM complex $\mathbf{C_1}$ for 1 h in 37 °C in a CO_2 incubator. After incubation, cells were washed several times with 1× PBS under dark conditions. Cells were then stained with DAPI in Vecta shield and observed under a fluorescence microscope.

3. RESULTS AND DISCUSSION

3.1. Synthesis and Characterization. As delineated in the Introduction, the first task of the present study was to synthesize a group of arene−ruthenium complexes using the chosen guanidine-based ancillary ligands ($\mathbf{L_1}$−$\mathbf{L_3}$). Accordingly, reactions of these ligands ($\mathbf{L_1}$−$\mathbf{L_3}$) with [{Ru(*p*-cymene)Cl_2}$_2$] were carried out in 5:1 methanol/dichloromethane, which furnished the desired complexes of type [Ru(*p*-cymene)(L)Cl]Cl in decent yields. The three complexes obtained with ligands $\mathbf{L_1}$, $\mathbf{L_2}$, and $\mathbf{L_3}$ are depicted, respectively, as $\mathbf{C_1}$, $\mathbf{C_2}$, and $\mathbf{C_3}$. Preliminary characterization (microanalysis, mass, IR, and NMR) data of these complexes agreed well with their compositions. In order to ascertain the coordination mode of the guanidine-based ligands in these complexes, the crystal structure of $\mathbf{C_3}$ was determined by X-ray crystallography.[21] The structure is presented in Figure 1, and

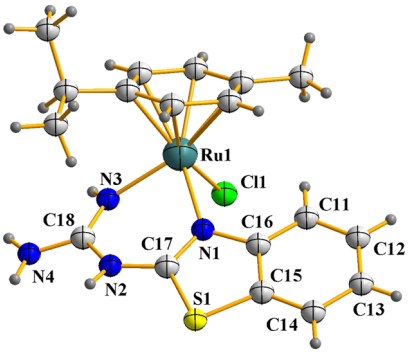

Figure 1. Crystal structure of the [Ru(*p*-cymene)($\mathbf{L_3}$)Cl]$^+$ complex.

some selected bond distances and angles are provided in Table 2. The structure reveals that the guanidine-based ligand ($\mathbf{L_3}$) is

Table 2. Selected Bond Distances and Bond Angles of Complex $\mathbf{C_3}$

Bond Distances (Å)			
Ru1−Cl1	2.4309(16)	N2−C18	1.377(8)
Ru1−N1	2.106(4)	N3−C18	1.308(8)
Ru1−N3	2.074(5)	N4−C18	1.340(9)
N1−C16	1.406(8)	S1−C15	1.734(7)
N1−C17	1.316(7)	S1−C17	1.739(6)
N2−C17	1.356(8)		
Bond Angles (deg)			
N1−Ru1−N3	82.83(19)	Cl1−Ru1−N1	86.13(16)
		Cl1−Ru1−N3	88.50(17)

https://doi.org/10.1021/acsomega.0c06265
ACS Omega 2021, 6, 8226−8238

coordinated to ruthenium as a neutral N,N-donor, forming a six-membered chelate ring (**I**, X = S and M = Ru) with a bite angle of ∼83°. The Ru($\mathbf{L}_3$) fragment of the complex is found to be nearly planar, as envisaged. The *p*-cymene moiety is bound to ruthenium in the usual π-fashion, and a chloride ion has taken up the sixth coordination site on the metal center. Another isolated chloride ion was located outside the coordination sphere. The bond parameters around ruthenium and within the coordinated organic ligands are all found to be quite usual.[3,9] Based on the similarity of the synthetic method and properties (vide infra), the other two complexes ($\mathbf{C}_1$ and $\mathbf{C}_2$) are assumed to have similar structures as $\mathbf{C}_3$.

3.2. Spectral Studies. Magnetic susceptibility measurements show that the $\mathbf{C}_1$−$\mathbf{C}_3$ complexes are diamagnetic, which is consistent with the +2 oxidation state of ruthenium (low-spin d^6 $S = 0$) in them. In the ^{1}H NMR spectra of the complexes, signals from both the coordinated *p*-cymene and guanidine-based ligand were expected, majority of which could be identified. For example, all the signals for the *p*-cymene ligand could be distinctly observed in all three complexes. Three signals from the alkyl groups are observed within 1.1−3.5 ppm and two signals from the aromatic fragment are observed within 5.2−5.8 ppm. From the guanidine-based ligands, the NH and NH_2 signals appeared within 6.5−8.2 ppm, while signals from the aromatic protons are observed around 7.5 ppm. In complex $\mathbf{C}_1$, a broad signal is observed at 10.50 ppm, which is absent in the spectra of the other two complexes, and hence, it is attributable to the benzimidazole-NH in metal-bound $\mathbf{L}_1$. ^{13}C NMR spectra of the complexes are also found to be consistent with their compositions. For the *p*-cymene ligand, three signals from the alkyl carbons are found below 40 ppm and four from the aromatic carbons appear within 70−90 ppm. For the guanidine-based ligands, two signals are observed above 150 ppm and signals from the phenyl ring are found within 110−130 ppm.

The mass spectra of complexes $\mathbf{C}_1$−$\mathbf{C}_3$, recorded in the positive ion mode, provide proof of coordination of the guanidine-based ligands. Each complex shows a peak at a *m*/*z* value that corresponds to the $[Ru(p\text{-cymene})(L\text{-}H)]^+$ fragment, which is generated via loss of HCl from the cationic $[Ru(p\text{-cymene})(L)Cl]^+$ unit. Associated with loss of the coordinated chloride ion, loss of proton is believed to take place from the central −NH− moiety of the guanidine-based ligand. This particular proton in such ligands is known to undergo facile dissociation.[22] Elimination of one equivalent HCl from compositionally similar arene−ruthenium complexes is precedent.[22] A similar mass spectral behavior of complexes $\mathbf{C}_1$−$\mathbf{C}_3$ supports their similar composition and structure.

Infrared spectra of complexes $\mathbf{C}_1$−$\mathbf{C}_3$, recorded in the 450−4000 cm^{-1} region, exhibit several bands. Upon comparison of the spectrum of each complex with that of the starting $[\{Ru(p\text{-cymene})Cl_2\}_2]$ complex reveals the presence of several new bands (near 3400, 3180, 1680, 1615, 1256, and 752 cm^{-1}) in the spectra of the complexes, which are attributable to the coordinated guanidine-based ligand. Among these bands, the two near 3400 and 3180 cm^{-1} are attributable to the −NH− and $-NH_2$ fragments, respectively. The NMR and IR data are therefore in good agreement with the composition of the complexes.

The $\mathbf{C}_1$−$\mathbf{C}_3$ complexes are soluble in polar solvents, such as water, methanol, ethanol, dimethylformamide, and dimethylsulfoxide, producing yellow solutions. Electronic spectra of the complexes were recorded in methanol solutions. Spectral data are presented in Table 3. Each complex shows four absorptions spanning the visible and ultraviolet regions. To have an insight into the nature of these absorptions, TDDFT calculations have been performed on the $\mathbf{C}_1$−$\mathbf{C}_3$ complexes, using the Gaussian 09 package,[11] and the results are found to be similar for all the complexes. The DFT-optimized structures of the complexes are shown in Figure S1 (Supporting Information) and some computed bond parameters are listed in Table S1 (Supporting Information). The computed bond parameters in the DFT-optimized structure of $\mathbf{C}_3$ are comparable with those found in its crystal structure. The main calculated transitions for the $\mathbf{C}_1$−$\mathbf{C}_3$ complexes and compositions of the molecular orbitals associated with the transitions are presented in Tables S2−S7 (Supporting Information), and contour plots of selected molecular orbitals are shown in Figure S2 (Supporting Information). As the computed optical transitions and compositions of the participating orbitals are similar for all three complexes, the case of $\mathbf{C}_1$ is described here as representative. Plots of experimental and theoretical spectra for $\mathbf{C}_1$ are deposited in Figure S3 (Supporting Information). The close match between each set of experimental and theoretical spectra testifies validity of the optimized structures of the complexes, particularly of complexes $\mathbf{C}_1$ and $\mathbf{C}_2$, for which crystal structures remained elusive. The lowest energy absorption at 451 nm is attributable primarily to a HOMO − 1 → LUMO transition, with much less HOMO − 3 → LUMO, HOMO − 2 → LUMO and HOMO → LUMO character. Additionally, based on the nature of the participating orbitals, the electronic excitation is best described as a MMCT transition mixed with some MLCT, LMCT, and LLCT character. The next absorption at 294 nm is mostly due to a HOMO − 1 → LUMO + 2 transition and assignable primarily to a MLCT transition with much less LLCT and ILCT character. The third absorption at 237 nm is largely due to a HOMO − 3 → LUMO + 2 transition and has a dominant MLCT character. The fourth absorption at 211 nm has a dominant HOMO − 3 → LUMO + 4 character and is assignable to a MLCT transition with some LLCT character.

Table 3. Electronic Absorption and Emission Spectral Data of the Complexes

	absorption spectral data[a]	emission spectral data[a]	
complex	λ_{max}, nm (ε, M^{-1} cm^{-1})	λ_F, nm [$\Phi_F \times 10^{-3}$][c]	life time (τ)
$\mathbf{C}_1$	451(400), 294 (5940), 237[b], 211 (21,970)	518 [8.6]	τ_1 = 0.26 ns, τ_2 = 4.10 ns
$\mathbf{C}_2$	449 (530), 282 (9190), 239[b], 209 (22,770)	558 [6.5]	τ_1 = 1.75 ns
$\mathbf{C}_3$	429 (490), 289 (7780), 255[b], 220 (28,780)	486 [17.3]	τ_1 = 0.36 ns, τ_2 = 5.02 ns

[a]In methanol. [b]Shoulder. [c]Quantum yield was calculated with reference to $[Ru(bpy)_3]^{2+}$ (Φ_F = 0.09).

Luminescence property of the complexes was examined in methanol solution. All three complexes were found to show prominent emission when excited near 400 nm (Table 3). It is interesting to note that the complexes absorb and emit in the visible region, a property much sought after in an antitumor agent for its easy identification in a biological matrix.

3.3. DNA Binding Studies. The interaction of the calf thymus DNA with complex $\mathbf{C}_1$, a representative of this family of complexes, was studied in detail to assess its potential as an antitumor agent. Initially, titration of the uncoordinated

https://doi.org/10.1021/acsomega.0c06265
ACS Omega 2021, 6, 8226−8238

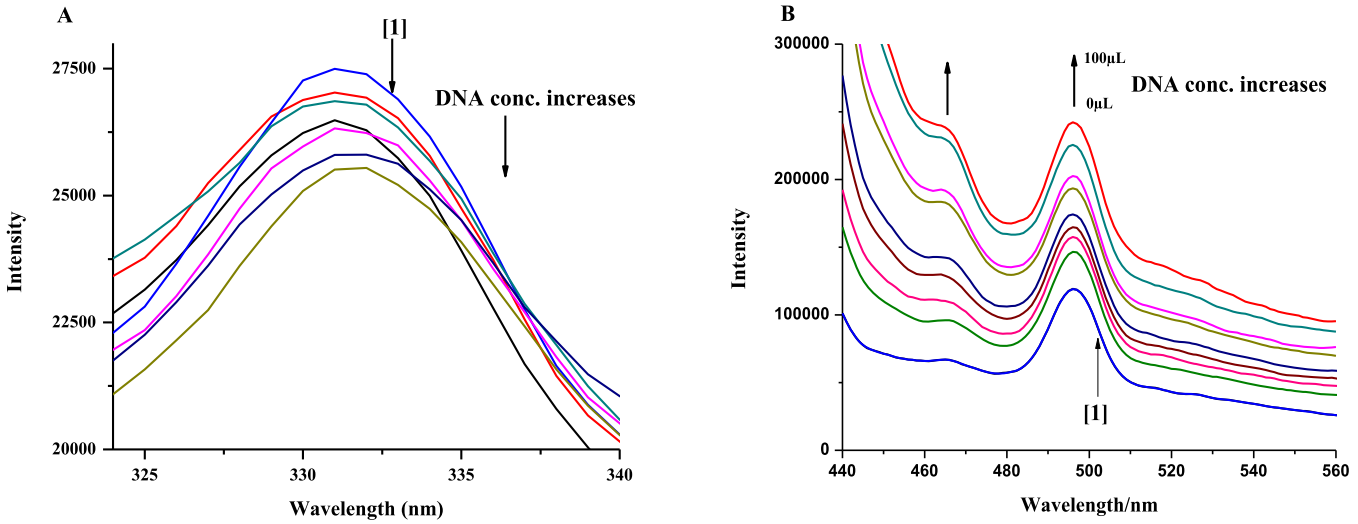

Figure 2. Fluorescence emission spectra of (A) 50 μM $\mathbf{L_1}$ and (B) 50 μM $\mathbf{C_1}$ in aqueous solution in the presence of 0.12 M NaCl and 30 mM Tris buffer (pH 7.4) in the absence (1) and presence of different concentrations of calf thymus DNA; temperature = 300 K.

Table 4. Binding Constant Values Obtained for the Interaction of Ligand $\mathbf{L_1}$ and Complex $\mathbf{C_1}$ with the Calf Thymus DNA that was Followed by Fluorescence Spectroscopy

		K_{app}				$K^* = K_{app} \times n_b$				
compound	expt	from double-reciprocal plot (a)	from non-linear plot (b)	from double-reciprocal plot with y-intercept = 1(c)	site size n_b	from double-reciprocal plot (a)	from non-linear plot (b)	from double-reciprocal plot with y-intercept = 1(c)	K^* from Scatchard	n_b from Scatchard as $n_b = (n^{-1})$
$\mathbf{L_1}$	1	2.80×10^3	3.30×10^3	1.60×10^3	8	2.20×10^4	2.60×10^4	1.28×10^4	1.86×10^4	8
	2	2.20×10^3	2.80×10^3	2.20×10^3	9	1.98×10^4	2.50×10^4	1.98×10^4	3.60×10^4	7
$\mathbf{C_1}$	1	0.94×10^4	0.80×10^4	0.70×10^4	13	1.20×10^4	1.04×10^4	0.91×10^4	1.53×10^4	15
	2	1.60×10^3	1.04×10^3	0.78×10^3	14	2.20×10^4	1.40×10^4	1.09×10^4	2.15×10^4	14

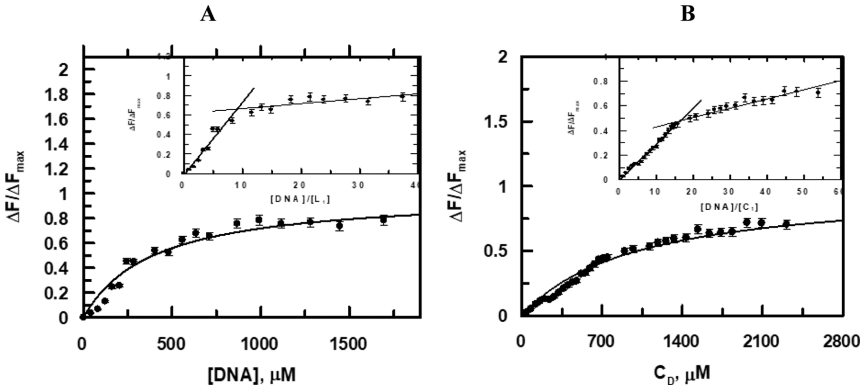

Figure 3. Binding isotherms for (A) ligand $\mathbf{L_1}$ and (B) complex $\mathbf{C_1}$ binding to the calf thymus DNA at pH ~ 7.4 and an ionic strength of 0.12 M. Corresponding non-linear fits are shown for these titrations that evaluate K_{app}. Inset: plot of the normalized increase in fluorescence as a function of the ratio of the calf thymus DNA to (A) ligand $\mathbf{L_1}$ and (B) complex $\mathbf{C_1}$. $[\mathbf{L_1}] = [\mathbf{C_1}] = 50$ μM, pH = 7.40, T = 300 K.

guanidine-based ligand $\mathbf{L_1}$ was carried out with the calf thymus DNA. Figure 2A shows a typical plot of this titration at the ionic strength and pH mentioned. Figure 2B is a similar plot for a titration performed with complex $\mathbf{C_1}$. The plots show that saturation is achieved in the binding of the compounds with DNA. Representative plots based on eq 2 are shown in Figure S4 (Supporting Information), from which the apparent binding constant (K_{app}) was evaluated (Table 4).[13−18] Plots in Figure 3A,B were fitted by the non-linear square fit analysis that also helps to evaluate K_{app}. Different binding parameters are shown in Table 4. The inset of Figure 3A,B provides n_b, the number of nucleotides bound to each compound (Table 4).[13−18] It is worth mentioning that the value for n_b obtained in the case of the complex binding to the calf thymus DNA was approximately 1.5 times greater than that obtained when the guanidine-based ligand $\mathbf{L_1}$ binds to the same DNA, suggesting that the complex engages more nucleic acid bases when it interacts with DNA, thus being able to bring about more distortion in DNA, an outcome of enforced planarity of the guanidine portion of the ligand following chelation to ruthenium (Table 4).[15,16,18]

Utilizing K_{app} and n_b from Table 4 and the relation $K_{app} \times n_b = K'$, the overall binding constants could be evaluated for the uncoordinated guanidine-based ligand $\mathbf{L_1}$ and complex

https://doi.org/10.1021/acsomega.0c06265
ACS Omega 2021, 6, 8226−8238

C_1.[13−18] Overall binding constants were also obtained from a modified version of the original Scatchard equation (eq 5),[19] and plots obeying this equation are shown in Figure S5 (Supporting Information). The overall binding constant values from the Scatchard equation were strikingly similar to those evaluated by multiplying K_{app} with n_b (eqs 2 and 4).

An interesting aspect regarding titration of the complex with the calf thymus DNA, followed by fluorescence spectroscopy, was that with an increase in the concentration of DNA (Figure 4), there was a gradual increase in fluorescence similar to that

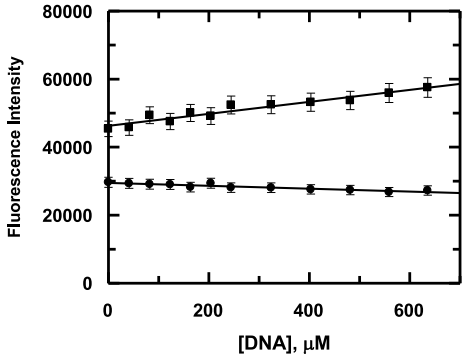

Figure 4. Gradual variation in fluorescence observed for the compounds as the calf thymus DNA was added during titration; (■) complex C_1, (●) ligand L_1. Ionic strength of medium = 0.12 M; pH ∼ 7.4; $[L_1] = [C_1] = 50\ \mu M$; temperature = 300 K.

observed for compounds including ethidium bromide that are known to intercalate DNA.[23−26] Hence, a logical conclusion is that the complex too is able to intercalate DNA, registering an increase in fluorescence. Such an increase in fluorescence upon interactions is an important attribute of the complex that may be utilized in a number of biological experiments to realize possible interactions of the compound with a biological target.

3.4. Molecular Docking with DNA. To elucidate the mode of interaction and binding affinity, docking studies were performed on B-DNA (PDB ID: 1BNA) in the presence of all the three complexes. The results show that the complexes interact with DNA quite similarly via the electrostatic mode. This is illustrated in Figure 5 for complex C_1 and in Figures S6 and S7 (Supporting Information) for complexes C_2 and C_3, respectively. In each case, the guanidine-based ligand is observed to form H-bonds with oxygen atoms of the phosphate backbone and also with the N3 atom of adenine of a single DNA strand. Additional H-bonding is observed in

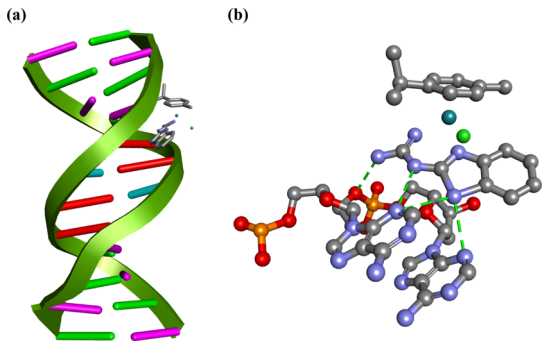

Figure 5. (a) Complex C_1 interacted with the DNA strand and (b) core view of the interaction (ball and stick model).

complex C_1 due to the presence of an NH fragment in L_1 that is absent in L_2 or L_3. The coordination-induced planarity of the guanidine-based ligands is found to favor strong H-bonding interactions, with better match of the complexes inside DNA strands allowing partial intercalation. Due to the combined effect of the van der Waals and H-bonding interactions, the complexes fit comfortably into the minor groove of the targeted DNA near the A−T rich regions.

Docking of the individual guanidine-based ligands with DNA has also been looked into. From the docked structures (Figure S8; Supporting Information), it is observed that the L_1 ligand shows the highest binding affinity to DNA, which is attributable to additional H-bonding possible due to the presence of an NH fragment in L_1, instead of oxygen (in L_2) or sulfur (in L_3). The same trend is observed in the complexes, which is also manifested in the biological studies. It is interesting to note that while all the uncoordinated guanidine-based ligands preferred to approach the G−C base pairs, upon binding to the metal center, the A−T base pairs have become their preferred binding location. Planarity of the guanidine-based ligands in the complexes and the presence of the Ru-coordinated *p*-cymene probably have caused this observed variation in their binding preference.

3.5. Cytotoxicity Studies. Cisplatin shows a remarkable efficacy in treating prostate cancer and has been quite successfully and extensively used in the last few decades.[27−29] However, as delineated in the Introduction, ruthenium-based molecular species, particularly the half-sandwich ruthenium−arene complexes, are also attracting attention owing to their demonstrated anticancer activities with minimal side effects. Encouraged by the prominent DNA binding properties of our three complexes (C_1, C_2, and C_3), we also determined the potency of these three complexes and cisplatin on the human prostate cancer cell line PC3 and the human benign prostate tumor cell line BPH1. Similarly, we have evaluated the toxic effect of these three complexes and cisplatin on the lung cancer cell line A549 and the normal lung fibroblast cell line WI-38. Cells were treated with three complexes (C_1, C_2, and C_3) in the concentration range of 0−100 μM for 24 h, followed by MTT assay. The results are displayed in Figure 6. Complex C_1 was found to be the most cytotoxic to PC3 cells ($IC_{50} = 39.5 \pm 1.57\ \mu M$) among the three complexes (Figure 6A). Complex C_1 was found to be non-toxic to the human prostate benign tumor cell line BPH1 even after 24 h of treatment, which suggests no side effects of it on non-carcinoma cells in our body. In this context, it is worth mentioning that cisplatin shows comparable cytotoxicity toward both PC3 and BPH1 cell lines. In A549 and WI-38 cell lines, C_1 shows moderate (IC_{50} values 69.4 ± 1.2 and 69.6 ± 3.45) and almost comparable cytotoxicity like cisplatin (IC_{50} values 60.1 ± 2.43 and 66.5 ± 2.12). Guanidine-based ligands (L_1, L_2, and L_3) have no cytotoxicity toward any type of cell lines, which signifies the effect of their coordination to ruthenium in antiproliferative activity. Figure 6B shows the % cell survival comparison between BPH1 and PC3 with C_1 complex for 24 h. The IC_{50} doses for all the complexes and cisplatin are summarized in Table 5. Interestingly, it was observed that the complexes could not exert significant toxicity toward A549 and WI-38. Among the different cells we have tested, only PC3 is PTEN-negative. Thus, it is reasonable to state that cytotoxicity generated through the compounds is presumably governed by nonfunctional PTEN. Similar results are also found in the case

https://doi.org/10.1021/acsomega.0c06265
ACS Omega 2021, 6, 8226−8238

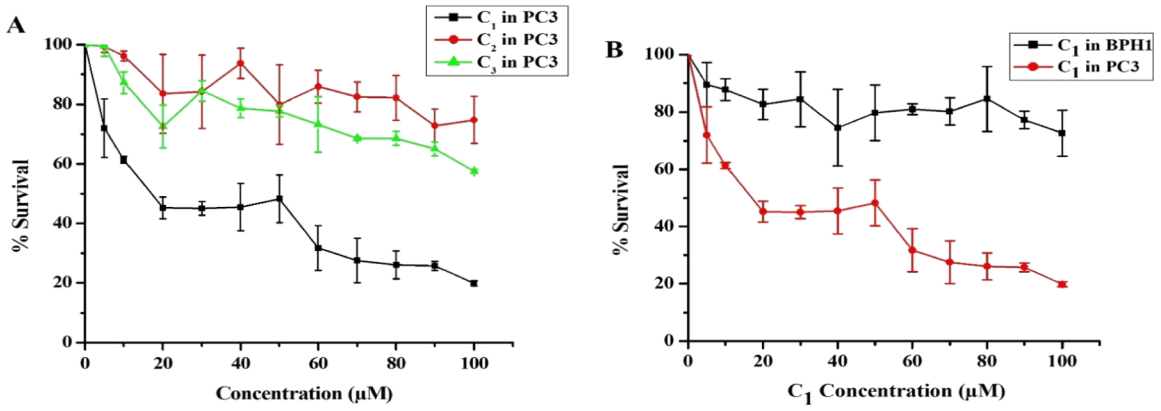

Figure 6. (A) MTT assay on the PC3 cell line after 24 h of treatment with three separate complexes C_1–C_3. (B) MTT assay on PC3 and BPH1 cell lines after 24 h of treatment with the C_1 complex. Data are presented as % survival relative to the untreated control. They are the mean ± SD of three independent experiments.

Table 5. IC_{50} Values of Ligands (L) and Complexes toward Different Cell Lines[a]

complex	PC3	BPH1	A549	WI-38	R_1[b]	R_2[c]
L_1	121.0 ± 1.57	>500 ± 4.5	>200 ± 2.2	>500 ± 4.67	nd	nd
L_2	168.8 ± 1.9	>500 ± 4.09	167.4 ± 1.77	>500 ± 5.03	nd	nd
L_3	446.4 ± 1.05	>500 ± 2.32	>200 ± 1.86	>500 ± 4.41	nd	nd
C_1	39.5 ± 1.57	263.0 ± 1.87	69.4 ± 1.2	69.6 ± 3.45	6.6	1.0
C_2	267.3 ± 2.01	443.9 ± 1.04	168.6 ± 1.5	135.9 ± 3.21	1.6	0.8
C_3	125.0 ± 1.43	175.2 ± 1.88	112.2 ± 1.9	135.7 ± 4.89	1.4	1.2
cisplatin	5.4 ± 1.93	8.0 ± 1.03	60.1 ± 2.43	66.5 ± 2.12	1.4	1.1

[a]The drug treatment period was 24 h. [b]R_1 = IC_{50} ratio of BPH1 cells to PC3 cells. [c]R_2 = IC_{50} ratio of WI-38 cells to A549 cells.

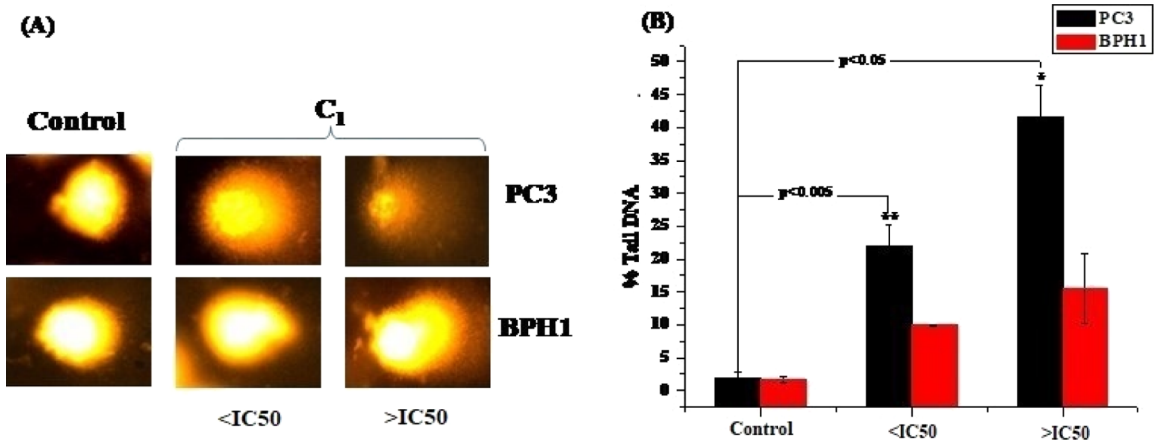

Figure 7. (A) Representative images of the comet assay of PC3 and BPH1 cell lines treated with the C_1 complex with respect to the untreated control. (B) Histogram shows % of comet tail DNA for PC3 and BPH1 cells treated with the C_1 complex for 24 h with respect to their untreated control at two different doses (<IC_{50} and >IC_{50} doses of PC3). Values are the mean ± SD of three independent experiments. *($p < 0.005$) and **($p < 0.005$) denote the statistically significant difference compared to the untreated control.

of curcumin.[30] All the other biological studies were done on two cell lines, PC3 and BPH1, taking C_1 as a model complex.

The cytotoxic effect of the C_1 complex is most likely linked to the DNA-damaging effects of the compound, and hence, we performed comet assay, a very useful and sensitive experiment for elucidating single- or double-strand DNA damage caused by any exogenous or endogenous species.[31] A small amount of nuclides/cells is required to perform this experiment and the tail length is considered to represent the level of DNA damage.[32] As shown in Figure 7A, the C_1 complex caused significantly ($p < 0.05$) more DNA damage at a concentration <IC_{50} or >IC_{50} dose in the case of PC3. However, at the same concentrations, no significant ($p > 0.05$) DNA damage was observed when BPH1 is used. Consistent with these data, the percentage of tail DNA increased significantly ($p < 0.05$) for C_1 complex-treated PC3 cells after 24 h of treatment (Figure 7B).

Nuclear morphology and the nature of cell death were studied by DAPI staining. The fluorescence micrographs of DAPI-stained PC3 and BPH1 cell lines are shown in Figure 8A, and the percentage of apoptotic cells is presented graphically in Figure 8B. When PC3 cells were treated with the C_1 complex at a concentration >IC_{50} dose for 24 h, we

https://doi.org/10.1021/acsomega.0c06265
ACS Omega 2021, 6, 8226−8238

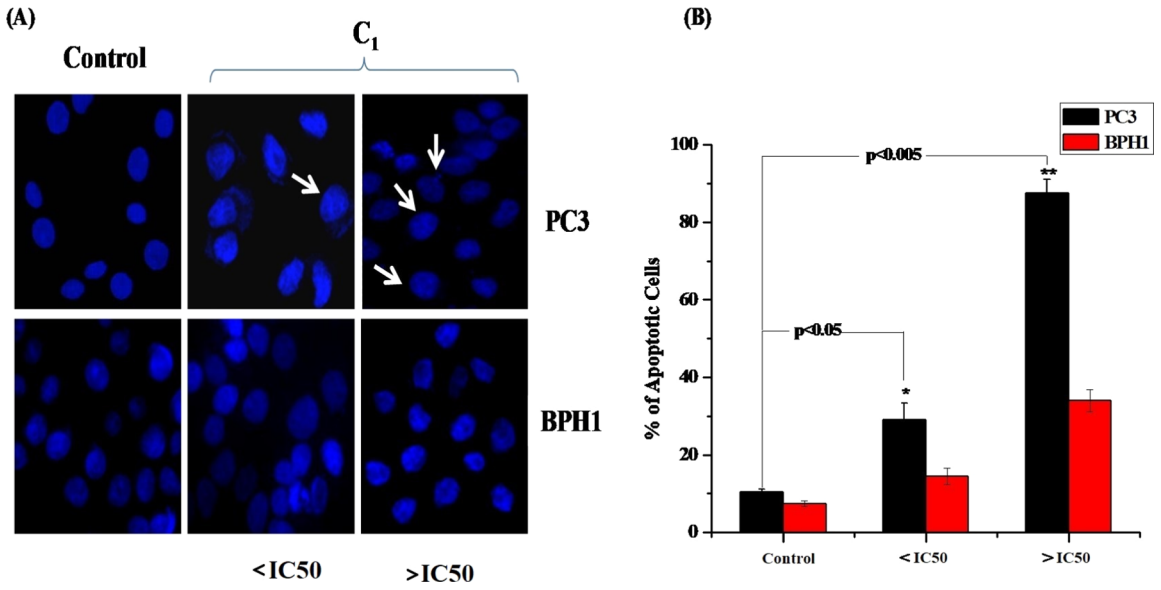

Figure 8. (A) Fluorescence micrographs of DAPI-stained PC3 and BPH1 cell lines under 40× magnification. Both the cells are treated with the C_1 complex for 24 h at two different doses (<IC_{50} and >IC_{50} doses of PC3). The arrow represents the decondensed nucleus of the apoptotic cells. (B) % of apoptotic cells as determined by DAPI staining followed by fluorescence microscopic observations. Each value represents the mean ± S.D. of three independent experiments. *($p < 0.05$) and **($p < 0.005$) denote the statistically significant difference compared to the untreated control.

found that 80−85% cells were apoptotic in nature, whereas for BPH1, the amount of apoptotic cells reduced to only 30−35%.

Ru(II)−arene complexes are well known to bring about cell damage via production of ROS within the cells.[33] It is interesting to note that among the other metals (such as Pt, Pd, and Au) used as therapeutics, only Ru shows higher antitumor activity mediated by an enhanced ROS production.[34] Apoptotic cell death and DNA damage are connected with ROS production, and we also estimated ROS production induced by the C_1 complex in PC3 and BPH1, where we have used a fluorescent dye, DCFDA (2′,7′-dichlorofluorescin diacetate), for indicating oxidative stress and hydroxyl and peroxyl radical generation.[35] The ROS generation in PC3 and BPH1 cell lines after treating with the C_1 complex for 24 h is shown in Figure 9. It was observed that PC3 cells exposed to the C_1 complex produced a significantly high amount ($p < 0.005$) of ROS, compared to BPH1 cells. The intracellular imaging behavior of the C_1 complex was studied in both PC3 and BPH1 cell lines using fluorescence microscopy, and the results obtained are illustrated in Figure 10. After incubation with the C_1 complex, BPH1 cells display no intracellular fluorescence. However, PC3 shows green fluorescence both in the cytoplasm and nuclei, suggesting that the C_1 complex was distributed both in the cytosol and nucleus in the proliferating cancer cell line.

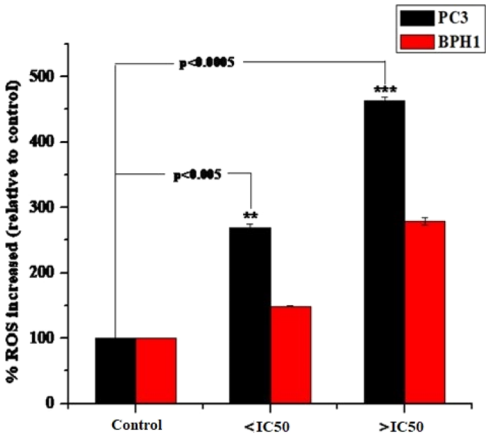

Figure 9. Intracellular ROS generation of PC3 and BPH1 cell lines treated with the C_1 complex for 24 h at two different doses (<IC_{50} and >IC_{50} doses of PC3). Data are presented as % increase in ROS relative to untreated controls. Values are the mean ± SD of three independent experiments. ***($p < 0.0005$) and ** ($p < 005$) denote the statistically significant difference compared to untreated controls.

4. CONCLUSIONS

The present study shows that the guanidine-based ligands (L) undergo facile reaction with [{Ru(*p*-cymene)Cl_2}$_2$] to furnish cationic half-sandwich complexes of type [Ru(*p*-cymene)(L)-Cl]$^+$. This study also reveals that the complexes are better DNA binders than the corresponding uncoordinated guanidine-based ligands, and the observed enhancement in DNA binding is attributable to the imposed planarity of the guanidine-based ligand upon coordination to ruthenium that enabled it to serve as a better intercalator. Cytotoxicity studies also show a similar trend, the complexes being more cytotoxic than the uncoordinated guanidine-based ligands, presumably because complex formation leads to an improvement in cellular uptake that permits more molecules to enter cells, showing greater cytotoxicity. The other important aspect is that compared to cancer cells, the complexes were found to be significantly less toxic to normal cells, and this is most prominent in the C_1 complex. This is probably due to the increased uptake of the complex molecules in cancer cells than normal cells, as the membrane transport system of cancer cells is more active than that of the normal cells or benign cells. Additionally, more uptake of complex molecules generates more reactive oxygen species that lead to more oxidative DNA damage as observed by the comet assay.[36] This study also demonstrates that inclusion of the guanidine-based ligands in the half-sandwich ruthenium−arene complexes, particularly in the C_1 complex, has been useful for exhibition of remarkable

https://doi.org/10.1021/acsomega.0c06265
ACS Omega 2021, 6, 8226−8238

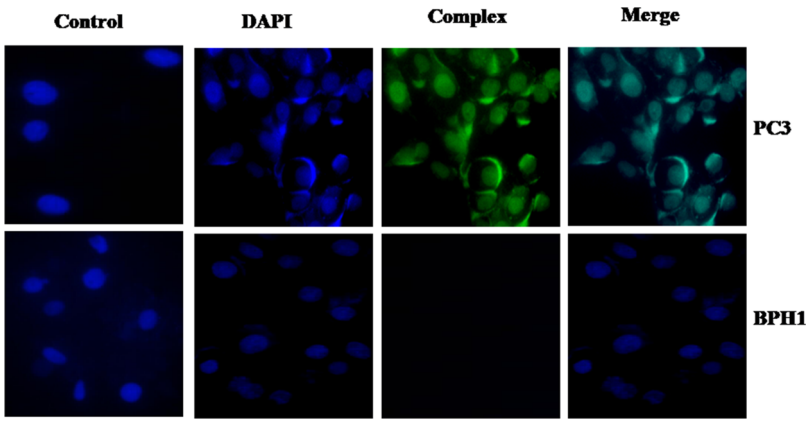

Figure 10. Cellular imaging of the C_1 complex in both PC3 and BPH1 cell lines under a fluorescence microscope. DAPI and the C_1 complex are visible as blue and green fluorescence, respectively. BPH1 cells display no intracellular fluorescence but PC3 shows green fluorescence both in the cytoplasm and nuclei.

antiproliferative activity against cancer cells with high selectivity and also for convenient tracing of the complexes in cells due to their prominent emissive nature. It is worth highlighting that such studies involving ligand modification at a single point (NH vs O vs S) are rare in the literature.[37]

■ ASSOCIATED CONTENT

Supporting Information

The Supporting Information is available free of charge at https://pubs.acs.org/doi/10.1021/acsomega.0c06265.

DFT-optimized structures and computed bond parameters; data and figures related to TDDFT calculations; and figures and tables related to biological studies (PDF)

Crystallographic data (CIF)

Accession Codes

CCDC 1955587 contains the supplementary crystallographic data for this paper.

■ AUTHOR INFORMATION

Corresponding Author

Samaresh Bhattacharya − *Department of Chemistry, Inorganic Chemistry Section, Jadavpur University, Kolkata 700 032, India;* orcid.org/0000-0002-6245-9752; Email: samaresh_b@hotmail.com

Authors

Jit Karmakar − *Department of Chemistry, Inorganic Chemistry Section, Jadavpur University, Kolkata 700 032, India*

Promita Nandy − *Department of Chemistry, Inorganic Chemistry Section, Jadavpur University, Kolkata 700 032, India*

Saurabh Das − *Department of Chemistry, Inorganic Chemistry Section, Jadavpur University, Kolkata 700 032, India;* orcid.org/0000-0002-0455-8760

Debalina Bhattacharya − *Department of Life Science and Biotechnology, Jadavpur University, Kolkata 700 032, India; Department of Microbiology, Maulana Azad College, Kolkata 700 013, India*

Parimal Karmakar − *Department of Life Science and Biotechnology, Jadavpur University, Kolkata 700 032, India*

Complete contact information is available at: https://pubs.acs.org/10.1021/acsomega.0c06265

Notes

The authors declare no competing financial interest.

■ ACKNOWLEDGMENTS

Financial assistance received from the JU-RUSA 2.0 program (ref. no.: R-11/438/19 (S.D.); R-11/76/19 (P.K.); R-11/96/19 (S.B.)) is gratefully acknowledged. The UGC-CAS, DST-FIST, and DST-PURSE programs of the Department of Chemistry, Jadavpur University, are also gratefully acknowledged for providing financial and infrastructural supports. P.K. acknowledges financial support from DST-SERB (EMR/2016/001151), Government of India. J.K. thanks CSIR, New Delhi, for his fellowship (grant no.: 09/096(0842)/2015-EMR-I). D.B. thanks the National Postdoctoral Fellowship Program of DST, Government of India, for her fellowship (grant no.: PDF/2017/001334).

■ REFERENCES

(1) (a) Soldevila-Barreda, J. J.; Metzler-Nolte, N. Intracellular Catalysis with Selected Metal Complexes and Metallic Nanoparticles: Advances toward the Development of Catalytic Metallodrugs. *Chem. Rev.* **2019**, *119*, 829−869. (b) Kenny, R. G.; Marmion, C. J. Toward Multi-Targeted Platinum and Ruthenium Drugs − A New Paradigm in Cancer Drug Treatment Regimens? *Chem. Rev.* **2019**, *119*, 1058−1137. (c) Thota, S.; Rodrigues, D. A.; Crans, D. C.; Barreiro, E. J. Ru(II) Compounds: Next-Generation Anticancer Metallotherapeutics? *J. Med. Chem.* **2018**, *61*, 5805−5821. (d) Meier-Menches, S. M.; Gerner, C.; Berger, W.; Hartinger, C. G.; Keppler, B. K. Structure-activity relationships for ruthenium and osmium anticancer agents − towards clinical development. *Chem. Soc. Rev.* **2018**, *47*, 909−928. (e) Zeng, L.; Gupta, P.; Chen, Y.; Wang, E.; Ji, L.; Chao, H.; Chen, Z.-S. The development of anticancer ruthenium(II) complexes: from single molecule compounds to nanomaterials. *Chem. Soc. Rev.* **2017**, *46*, 5771−5804. (f) Murray, B. S.; Babak, M. V.; Hartinger, C. G.; Dyson, P. J. The development of RAPTA compounds for the treatment of tumors. *Coord. Chem. Rev.* **2016**, *306*, 86−114. (g) Medici, S.; Peana, M.; Nurchi, V. M.; Lachowicz, J. I.; Crisponi, G.; Zoroddu, M. A. Noble metals in medicine: Latest advances. *Coord. Chem. Rev.* **2015**, *284*, 329−350. (h) Singh, A. K.; Pandey, D. S.; Xu, Q.; Braunstein, P. Recent advances in supramolecular and biological aspects of arene ruthenium(II) complexes. *Coord. Chem. Rev.* **2014**, *270*−*271*, 31−56. (i) Hartinger, C. G.; Metzler-Nolte, N.; Dyson, P. J. Challenges and Opportunities in the Development of Organometallic Anticancer Drugs. *Organometallics* **2012**, *31*, 5677−5685. (j) Gasser, G.; Ott, I.; Metzler-Nolte, N. Organometallic Anticancer Compounds. *J. Med. Chem.* **2011**, *54*, 3−25.

(2) (a) Li, H.; Xie, C.; Lan, R.; Zha, S.; Chan, C.-F.; Wong, W.-Y.; Ho, K.-L.; Chan, B. D.; Luo, Y.; Zhang, J.-X.; Law, G.-L.; Tai, W. C. S.; Bünzli, J.-C. G.; Wong, K.-L. A Smart Europium-Ruthenium Complex as Anticancer Prodrug: Controllable Drug Release and Real-Time Monitoring under Different Light Excitations. *J. Med. Chem.* **2017**, *60*, 8923−8932. (b) Martínez, M. Á.; Carranza, M. P.; Massaguer, A.; Santos, L.; Organero, J. A.; Aliende, C.; de Llorens, R.; Ng-Choi, I.; Feliu, L.; Planas, M.; Rodríguez, A. M.; Manzano, B. R.; Espino, G.; Jalón, F. A. Synthesis and Biological Evaluation of Ru(II) and Pt(II) Complexes Bearing Carboxyl Groups as Potential Anticancer Targeted Drugs. *Inorg. Chem.* **2017**, *56*, 13679−13696. (c) Qu, F.; Park, S.; Martinez, K.; Gray, J. L.; Thowfeik, F. S.; Lundeen, J. A.; Kuhn, A. E.; Charboneau, D. J.; Gerlach, D. L.; Lockart, M. M.; Law, J. A.; Jernigan, K. L.; Chambers, N.; Zeller, M.; Piro, N. A.; Kassel, W. S.; Schmehl, R. H.; Paul, J. J.; Merino, E. J.; Kim, Y.; Papish, E. T. Ruthenium Complexes are pH-Activated Metallo Prodrugs (pHAMPs) with Light-Triggered Selective Toxicity Toward Cancer Cells. *Inorg. Chem.* **2017**, *56*, 7519−7532. (d) Lenis-Rojas, O. A.; Roma-Rodrigues, C.; Fernandes, A. R.; Marques, F.; Pérez-Fernández, D.; Guerra-Varela, J.; Sánchez, L.; Vázquez-García, D.; López-Torres, M.; Fernández, A.; Fernández, J. J. Dinuclear RuII(bipy)2 Derivatives: Structural, Biological, and in vivo Zebrafish Toxicity Evaluation. *Inorg. Chem.* **2017**, *56*, 7127−7144. (e) Shen, J.; Kim, H.-C.; Wolfram, J.; Mu, C.; Zhang, W.; Liu, H.; Xie, Y.; Mai, J.; Zhang, H.; Li, Z.; Guevara, M.; Mao, Z.-W.; Shen, H. A Liposome Encapsulated Ruthenium Polypyridine Complex as a Theranostic Platform for Triple-Negative Breast Cancer. *Nano Lett.* **2017**, *17*, 2913−2920. (f) Heinemann, F.; Karges, J.; Gasser, G. Critical Overview of the Use of Ru(II) Polypyridyl Complexes as Photosensitizers in One-Photon and Two-Photon Photodynamic Therapy. *Acc. Chem. Res.* **2017**, *50*, 2727−2736.

(3) (a) Jeyalakshmi, K.; Haribabu, J.; Balachandran, C.; Swaminathan, S.; Bhuvanesh, N. S. P.; Karvembu, R. Coordination Behavior of N,N′,N″-Trisubstituted Guanidine Ligands in Their Ru-Arene Complexes: Synthetic, DNA/Protein Binding, and Cytotoxic Studies. *Organometallics* **2019**, *38*, 753−770. (b) Muralisankar, M.; Dheepika, R.; Haribabu, J.; Balachandran, C.; Aoki, S.; Bhuvanesh, N. S. P.; Nagarajan, S. Design, Synthesis, DNA/HSA Binding, and Cytotoxic Activity of Half-Sandwich Ru(II)-Arene Complexes Containing Triarylamine-Thiosemicarbazone Hybrids. *ACS Omega* **2019**, *4*, 11712−11723. (c) Sarkar, B.; Mondal, A.; Madaan, Y.; Roy, N.; Moorthy, A.; Kuo, Y.-C.; Paira, P. Luminescent anticancer ruthenium(II)-p-cymene complexes of extended imidazophenanthroline ligands: synthesis, structure, reactivity, biomolecular interactions and live cell imaging. *Dalton Trans.* **2019**, *48*, 12257−12271. (d) Yousuf, I.; Arjmand, F.; Tabassum, S.; Ahmad, M. Design and synthesis of a DNA intercalative half-sandwich organoruthenium(II)-chromone complex: cytotoxicity evaluation and topoisomerase Iα inhibition assay. *New J. Chem.* **2019**, *43*, 5475−5487. (e) Lari, M.; Martínez-Alonso, M.; Busto, N.; Manzano, B. R.; Rodríguez, A. M.; Acuña, M. I.; Domínguez, F.; Albasanz, J. L.; Leal, J. M.; Espino, G.; García, B. Strong Influence of Ancillary Ligands Containing Benzothiazole or Benzimidazole Rings on Cytotoxicity and Photoactivation of Ru(II) Arene Complexes. *Inorg. Chem.* **2018**, *57*, 14322−14336. (f) Lenis-Rojas, O. A.; Robalo, M. P.; Tomaz, A. I.; Carvalho, A.; Fernandes, A. R.; Marques, F.; Folgueira, M.; Yáñez, J.; Vázquez-García, D.; López Torres, M.; Fernández, A.; Fernández, J. J. RuII(p-cymene) Compounds as Effective and Selective Anticancer Candidates with No Toxicity in Vivo. *Inorg. Chem.* **2018**, *57*, 13150−13166. (g) Li, J.; Tian, M.; Tian, Z.; Zhang, S.; Yan, C.; Shao, C.; Liu, Z. Half-Sandwich Iridium(III) and Ruthenium(II) Complexes Containing P̂P-Chelating Ligands: A New Class of Potent Anticancer Agents with Unusual Redox Features. *Inorg. Chem.* **2018**, *57*, 1705−1716. (h) Paitandi, R. P.; Sharma, V.; Singh, V. D.; Dwivedi, B. K.; Mobin, S. M.; Pandey, D. S. Pyrazole appended quinoline-BODIPY based arene ruthenium complexes: their anticancer activity and potential applications in cellular imaging. *Dalton Trans.* **2018**, *47*, 17500−17514. (i) Mandal, P.; Kundu, B. K.; Vyas, K.; Sabu, V.; Helen, A.; Dhankhar, S. S.; Nagaraja, C. M.; Bhattacherjee, D.; Bhabak, K. P.; Mukhopadhyay, S. Ruthenium(II) arene NSAID complexes: inhibition of cyclooxygenase and antiproliferative activity against cancer cell lines. *Dalton Trans.* **2018**, *47*, 517−527. (j) Gopalakrishnan, D.; Ganeshpandian, M.; Loganathan, R.; Bhuvanesh, N. S. P.; Sabina, X. J.; Karthikeyan, J. Water soluble Ru(II)−arene complexes of the antidiabetic drug metformin: DNA and protein binding, molecular docking, cytotoxicity and apoptosis-inducing activity. *RSC Adv.* **2017**, *7*, 37706−37719. (k) Jeyalakshmi, K.; Haribabu, J.; Balachandran, C.; Bhuvanesh, N. S. P.; Emi, N.; Karvembu, R. Synthesis of Ru(II)-benzene complexes containing aroylthiourea ligands, and their binding with biomolecules and in vitro cytotoxicity through apoptosis. *New J. Chem.* **2017**, *41*, 2672−2686. (l) Barragán, F.; López-Senín, P.; Salassa, L.; Betanzos-Lara, S.; Habtemariam, A.; Moreno, V.; Sadler, P. J.; Marchán, V. Photocontrolled DNA Binding of a Receptor-Targeted Organometallic Ruthenium(II) Complex. *J. Am. Chem. Soc.* **2011**, *133*, 14098.

(4) (a) Ashraf, A.; Aman, F.; Movassaghi, S.; Zafar, A.; Kubanik, M.; Siddiqui, W. A.; Reynisson, J.; Söhnel, T.; Jamieson, S. M. F.; Hanif, M.; Hartinger, C. G. Structural Modifications of the Antiinflammatory Oxicam Scaffold and Preparation of Anticancer Organometallic Compounds. *Organometallics* **2019**, *38*, 361−374. (b) Swaminathan, S.; Haribabu, J.; Kalagatur, N. K.; Konakanchi, R.; Balakrishnan, N.; Bhuvanesh, N.; Karvembu, R. Synthesis and Anticancer Activity of [RuCl2(η6-arene)(aroylthiourea)] Complexes − High Activity against the Human Neuroblastoma (IMR-32) Cancer Cell Line. *ACS Omega* **2019**, *4*, 6245−6256. (c) Hager, L. A.; Mokesch, S.; Kieler, C.; Alonso-de Castro, S.; Baier, D.; Roller, A.; Kandioller, W.; Keppler, B. K.; Berger, W.; Salassa, L.; Terenzi, A. Ruthenium-arene complexes bearing naphthyl-substituted 1,3-dioxoindan-2-carboxamides ligands for G-quadruplex DNA recognition. *Dalton Trans.* **2019**, *48*, 12040−12049. (d) Sarkar, A.; Acharya, S.; Khushvant, K.; Purkait, K.; Mukherjee, A. Cytotoxic Ru^{II}-p-cymene complexes of an anthraimidazoledione: halide dependent solution stability, reactivity and resistance to hypoxia deactivation. *Dalton Trans.* **2019**, *48*, 7187−7197. (e) Laurent, Q.; Batchelor, L. K.; Dyson, P. J. Applying a Trojan Horse Strategy to Ruthenium Complexes in the Pursuit of Novel Antibacterial Agents. *Organometallics* **2018**, *37*, 915−923. (f) Gatti, A.; Habtemariam, A.; Romero-Canelón, I.; Song, J.-I.; Heer, B.; Clarkson, G. J.; Rogolino, D.; Sadler, P. J.; Carcelli, M. Half-Sandwich Arene Ruthenium(II) and Osmium(II) Thiosemicarbazone Complexes: Solution Behavior and Antiproliferative Activity. *Organometallics* **2018**, *37*, 891−899. (g) Zhao, J.; Zhang, D.; Hua, W.; Li, W.; Xu, G.; Gou, S. Anticancer Activity of Bifunctional Organometallic Ru(II) Arene Complexes Containing a 7-Hydroxycoumarin Group. *Organometallics* **2018**, *37*, 441−447. (h) Mu, C.; Prosser, K. E.; Harrypersad, S.; MacNeil, G. A.; Panchmatia, R.; Thompson, J. R.; Sinha, S.; Warren, J. J.; Walsby, C. J. Activation by Oxidation: Ferrocene-Functionalized Ru(II)-Arene Complexes with Anticancer, Antibacterial, and Antioxidant Properties. *Inorg. Chem.* **2018**, *57*, 15247−15261. (i) Lenis-Rojas, O. A.; Robalo, M. P.; Tomaz, A. I.; Carvalho, A.; Fernandes, A. R.; Marques, F.; Folgueira, M.; Yáñez, J.; Vázquez-García, D.; López Torres, M.; Fernández, A.; Fernández, J. J. RuII(p-cymene) Compounds as Effective and Selective Anticancer Candidates with No Toxicity in vivo. *Inorg. Chem.* **2018**, *57*, 13150−13166. (j) Ma, L.; Lin, X.; Li, C.; Xu, Z.; Chan, C.-Y.; Tse, M.-K.; Shi, P.; Zhu, G. A Cancer Cell-Selective and Low-Toxic Bifunctional Heterodinuclear Pt(IV)-Ru(II) Anticancer Prodrug. *Inorg. Chem.* **2018**, *57*, 2917−2924. (k) Shanmugaraju, S.; la Cour Poulsen, B.; Arisa, T.; Umadevi, D.; Dalton, H. L.; Hawes, C. S.; Estalayo-Adrián, S.; Savyasachi, A. J.; Watson, G. W.; Williams, D. C.; Gunnlaugsson, T. Synthesis, structural characterization and antiproliferative activity of a new fluorescent 4-amino-1,8-naphthalimide Tröger's base-Ru(II)-curcumin organometallic conjugate. *Chem. Commun.* **2018**, *54*, 4120−4123. (l) Batchelor, L. K.; Păunescu, E.; Soudani, M.; Scopelliti, R.; Dyson, P. J. Influence of the Linker Length on the Cytotoxicity of Homobinuclear Ruthenium(II) and Gold(I) Complexes. *Inorg. Chem.* **2017**, *56*, 9617−9633. (m) Guerriero, A.; Oberhauser, W.; Riedel, T.; Peruzzini, M.; Dyson, P. J.; Gonsalvi, L. New Class of Half-Sandwich Ruthenium(II) Arene Complexes Bearing the Water-Soluble CAP

https://doi.org/10.1021/acsomega.0c06265
ACS Omega 2021, 6, 8226−8238

Ligand as an in vitro Anticancer Agent. *Inorg. Chem.* **2017**, *56*, 5514−5518. (n) Mitra, R.; Samuelson, A. G. Mitigating UVA light induced reactivity of 6-thioguanine through formation of a Ru(II) half-sandwich complex. *RSC Adv.* **2014**, *4*, 24304−24306. Romero-Canelón, I.; Salassa, L.; Sadler, P. J. The Contrasting Activity of Iodido versus Chlorido Ruthenium and Osmium Arene Azo- and Imino-pyridine Anticancer Complexes: Control of Cell Selectivity, Cross-Resistance, p53 Dependence, and Apoptosis Pathway. *J. Med. Chem.* **2013**, *56*, 1291−1300. (p) Das, S.; Sinha, S.; Britto, R.; Somasundaram, K.; Samuelson, A. G. Cytotoxicity of half sandwich ruthenium(II) complexes with strong hydrogen bond acceptor ligands and their mechanism of action. *J. Inog. Biochem.* **2010**, *104*, 93−104.

(5) Novakova, O.; Chen, H.; Vrana, O.; Rodger, A.; Sadler, P. J.; Brabec, V. DNA Interactions of Monofunctional Organometallic Ruthenium(II) Antitumor Complexes in Cell-free Media. *Biochemistry* **2003**, *42*, 11544−11554.

(6) (a) Arkin, M. R.; Jenkins, Y.; Murphy, C. J.; Turro, N. J.; Barton, J. K. Metallointercalators as Probes of the DNA π-way. *Mechanistic Bioinorganic Chemistry*; American Chemical Society, 1996; Chapter 17, pp 449−469. (b) Elmes, R. B. P.; Ryan, G. J.; Erby, M. L.; Frimannsson, D. O.; Kitchen, J. A.; Lawler, M.; Williams, D. C.; Quinn, S. J.; Gunnlaugsson, T. Synthesis, Characterization, and Biological Profiling of Ruthenium(II)-Based 4-Nitro- and 4-Amino-1,8-naphthalimide Conjugates. *Inorg. Chem.* **2020**, *59*, 10874−10893. (c) Zhang, S.-Q.; Meng, T.-T.; Li, J.; Hong, F.; Liu, J.; Wang, Y.; Gao, L.-H.; Zhao, H.; Wang, K.-Z. Near-IR/Visible-Emitting Thiophenyl-Based Ru(II) Complexes: Efficient Photodynamic Therapy, Cellular Uptake, and DNA Binding. *Inorg. Chem.* **2019**, *58*, 14244−14259. (d) Abreu, F. D.; Paulo, T. d. F.; Gehlen, M. H.; Ando, R. A.; Lopes, L. G. F.; Gondim, A. C. S.; Vasconcelos, M. A.; Teixeira, E. H.; Sousa, E. H. S.; de Carvalho, I. M. M. Aryl-Substituted Ruthenium(II) Complexes: A Strategy for Enhanced Photocleavage and Efficient DNA Binding. *Inorg. Chem.* **2017**, *56*, 9084−9096.

(7) (a) Banerjee, D.; Pal, S. K. Excited-State Solvation and Proton Transfer Dynamics of DAPI in Biomimetics and Genomic DNA. *J. Phys. Chem. A* **2008**, *112*, 7314−7320. (b) Bourzac, K. M.; LaVine, L. J.; Rice, M. S. Analysis of DAPI and SYBR Green I as Alternatives to Ethidium Bromide for Nucleic Acid Staining in agarose Gel Electrophoresis. *J. Chem. Educ.* **2003**, *80*, 1292−1296. (c) Reha, D.; Kabelác, M.; Ryjácek, F.; Sponer, J.; Sponer, J. E.; Elstner, M.; Suhai, S.; Hobza, P. Intercalators. 1. Nature of Stacking Interactions between Intercalators (Ethidium, Daunomycin, Ellipticine, and 4′,6-Diaminide-2-phenylindole) and DNA Base Pairs. Ab Initio Quantum Chemical, Density Functional Theory, and Empirical Potential Study. *J. Am. Chem. Soc.* **2002**, *124*, 3366. (d) Lan, T.; McLaughlin, L. W. The Energetic Contribution of a Bifurcated Hydrogen Bond to the Binding of DAPI to dA-dT Rich Sequences of DNA. *J. Am. Chem. Soc.* **2001**, *123*, 2064−2065. (e) Vlieghe, D.; Sponer, J.; Meervelt, L. V. Crystal Structure of d(GGCCAATTGG) Complexed with DAPI Reveals Novel Binding Mode. *Biochemistry* **1999**, *38*, 16443−16451. (f) Albert, F. G.; Eckdahl, T. T.; Fitzgerald, D. J.; Anderson, J. N. Heterogeneity in the Actions of Drugs That Bind in the DNA Minor Groove. *Biochemistry* **1999**, *38*, 10135−10146.

(8) (a) Mohamed, S. K.; Soliman, A. M.; El-Remaily, M. A. A.; Abdel-Ghany, H. Eco Friendly Synthesis of Pyrimidine and Dihydropyrimidinone Derivatives under Solvent Free Condition and their Anti-microbial Activity. *Chem. Sci. J.* **2013**, *2013*, 1. (b) King, F. E.; Acheson, R. M.; Spensley, P. C. 275. Benziminazole analogues of paludrine. *J. Chem. Soc.* **1948**, *17*, 1366−1371.

(9) (a) Mukherjee, T.; Ganzmann, C.; Bhuvanesh, N.; Gladysz, J. A. Syntheses of Enantiopure Bifunctional 2-Guanidinobenzimidazole Cyclopentadienyl Ruthenium Complexes: Highly Enantioselective Organometallic Hydrogen Bond Donor Catalysts for Carbon-Carbon Bond Forming Reactions. *Organometallics* **2014**, *33*, 6723−6737. (b) Scherer, A.; Mukherjee, T.; Hampel, F.; Gladysz, J. A. Metal-Templated Hydrogen Bond Donors as "Organocatalysts" for Carbon-Carbon Bond Forming Reactions: Syntheses, Structures, and Reactivities of 2-Guanidinobenzimidazole Cyclopentadienyl Ruthenium Complexes. *Organometallics* **2014**, *33*, 6709−6722. (c) Sánchez-Guadarrama, O.; López-Sandoval, H.; Sánchez-Bartéz, F.; Gracia-Mora, I.; Höpfl, H.; Barba-Behrens, N. Cytotoxic activity, X-ray crystal structures and spectroscopic characterization of cobalt(II), copper(II) and zinc(II) coordination compounds with 2-substituted benzimidazoles. *J. Inorg. Biochem.* **2009**, *103*, 1204−1213. (d) Albada, G. A. v.; Turpeinen, U.; Reedijk, J. Two different isomers of tetrahedrally distorted square-planar Cu(II) triflate compounds with 2-guanidinobenzimidazole; synthesis, X-ray and spectroscopic characterisation. *J. Mol. Struct.* **2006**, *789*, 182−186. (e) Zheng, L.; Zhang, J.; Yu, M.-M.; Ni, Z.-H.; Kou, H.-Z. Bis(2 guanidinobenzimidazole-K^2 N, N')copper(II) bis(dicyanamide). *Acta Crystallogr., Sect. E: Struct. Rep. Online* **2006**, *62*, m2470−m2472. (f) Arablo, N.; Torabi, S. A. A.; Morsali, A.; Skelton, B. W.; White, A. H. Cation Structures in Bis(2-Guanidino-benzimidazole)metal(II) Complexes: Crystal and Molecular Structure of the Copper(II) Perchlorate Adduct. *Aust. J. Chem.* **2003**, *56*, 945−947. (g) Ceniceros-Gómez, A. E.; Barba-Behrens, N.; Quiroz-Castro, M. E.; Bernès, S.; Nöth, H.; Castillo-Blum, S. E. Synthesis, X-ray and spectroscopic characterisation of chromium(III) coordination compounds with benzimidazolic ligands. *Polyhedron* **2000**, *19*, 1821−1827. (h) Ceniceros-Gómez, A. E.; Barba-Behrens, N.; Bernès, S.; Nöth, H.; Castillo-Blum, S. E. Synthesis, X-ray and NMR characterisation of cobalt(III) coordination compounds with 2-guanidinobenzimidazole. *Inorg. Chim. Acta* **2000**, *304*, 230−236. (i) Barba-Behrens, N.; Vázquez-Olmos, A.; Castillo-Blum, S. E.; Höjer, G.; Meza-Höjer, S.; Hernández, R. M.; de Jesús Rosales-Hoz, M.; Vicente, R.; Escuer, A. Coordination behaviour of 2-guanidinobenzimidazole towards cobalt(II), nickel(II), copper(II) and zinc(II). An experimental and theoretical study. *Transition Met. Chem.* **1996**, *21*, 31−37.

(10) Bennett, M. A.; Huang, T. N.; Matheson, T. W.; Smith, A. K. *Inorg. Synth.* **1982**, *1*, 75.

(11) Frisch, M. J.; Trucks, G. W.; Schlegel, H. B.; Scuseria, G. E.; Robb, M. A.; Cheeseman, J. R.; Scalmani, G.; Barone, V.; Mennucci, B.; Petersson, G. A.; Nakatsuji, H.; Caricato, M.; Li, X.; Hratchian, H. P.; Izmaylov, A. F.; Bloino, J.; Zheng, G.; Sonnenberg, J. L.; Hada, M.; Ehara, M.; Toyota, K.; Fukuda, R.; Hasegawa, J.; Ishida, M.; Nakajima, T.; Honda, Y.; Kitao, O.; Nakai, H.; Vreven, T.; Montgomery, J. A., Jr.; Peralta, J. E.; Ogliaro, F.; Bearpark, M.; Heyd, J. J.; Brothers, E.; Kudin, K. N.; Staroverov, V. N.; Kobayashi, R.; Normand, J.; Raghavachari, K.; Rendell, A.; Burant, J. C.; Iyengar, S. S.; Tomasi, J.; Cossi, M.; Rega, N.; Millam, J. M.; Klene, M.; Knox, J. E.; Cross, J. B.; Bakken, V.; Adamo, C.; Jaramillo, J.; Gomperts, R.; Stratmann, R. E.; Yazyev, O.; Austin, A. J.; Cammi, R.; Pomelli, C.; Ochterski, J. W.; Martin, R. L.; Morokuma, K.; Zakrzewski, V. G.; Voth, G. A.; Salvador, P.; Dannenberg, J. J.; Dapprich, S.; Daniels, A. D.; Farkas, Ö.; Foresman, J. B.; Ortiz, J. V.; Cioslowski, J.; Fox, D. J. *Gaussian 9*; Gaussian, Inc.: Wallingford CT, 2009.

(12) Sheldrick, G. M. *SHELXS-97 and SHELXL-97, Fortran programs for crystal structure solution and refinement*; University of Göttingen: Göttingen, Germany, 1997. (b) Sheldrick, G. M. A short history of SHELX. *Acta Crystallogr., Sect. A: Found. Crystallogr.* **2008**, *64*, 112−122.

(13) Das, S.; Dasgupta, D. Binding of (MTR)2Zn2+ complex to chromatin: A comparison with $(MTR)_2Mg^{2+}$ complex. *J. Inorg. Biochem.* **2005**, *99*, 707−715.

(14) Roy, S.; Banerjee, R.; Sarkar, M. Direct binding of Cu(II)-complexes of oxicam NSAIDs with DNA backbone. *J. Inorg. Biochem.* **2006**, *100*, 1320−1331.

(15) Guin, P. S.; Das, S.; Mandal, P. C. Studies on the formation of a complex of Cu(II) with sodium 1,4-dihydroxy-9,10-anthraquinone-2-sulphonate − An analogue of the core unit of anthracycline anticancer drugs and its interaction with calf thymus DNA. *J. Inorg. Biochem.* **2009**, *103*, 1702−1710.

(16) Das, P.; Jain, C. K.; Dey, S. K.; Saha, R.; Chowdhury, A. D.; Roychoudhury, S.; Kumar, S.; Majumder, H. K.; Das, S. Synthesis, crystal structure, DNA interaction and *in vitro* anticancer activity of a Cu(II) complex of purpurin: dual poison for human DNA topoisomerase I and II. *RSC Adv.* **2014**, *4*, 59344−59357.

https://doi.org/10.1021/acsomega.0c06265
ACS Omega 2021, 6, 8226−8238

(17) Das, P.; Jain, C. K.; Roychoudhury, S.; Majumder, H. K.; Das, S. Design, synthesis and *in vitro* anticancer activity of a Cu(II) complex of carminic acid: A novel small molecule inhibitor of human DNA topoisomerase I and topoisomerase II. *ChemistrySelect* **2016**, *1*, 6623−6631.
(18) Mukherjee Chatterjee, S.; Jain, C. K.; Singha, S.; Das, P.; Roychoudhury, S.; Majumder, H. K.; Das, S. Activity of Co^{II}−Quinalizarin: A novel analogue of anthracycline-based anticancer agents targets human DNA topoisomerase, whereas quinalizarin itself acts via formation of semiquinone on acute lymphoblastic leukemia MOLT-4 and HCT 116 cells. *ACS Omega* **2018**, *3*, 10255−10266.
(19) Scatchard, G. The attractions of proteins for small molecules and ions. *Ann. N.Y. Acad. Sci.* **1949**, *51*, 660−672.
(20) Singh, N. P.; McCoy, M. T.; Tice, R. R.; Schneider, E. L. A simple technique for quantitation of low levels of DNA damage in individual cells. *Exp. Cell Res.* **1988**, *175*, 184−191.
(21) Attempts to grow single crystals of complexes $\mathbf{C_1}$ and $\mathbf{C_2}$ remained unsuccessful.
(22) Nikolić, S.; Opsenica, D. M.; Filipović, V.; Dojčinović, B.; Aranđelović, S.; Radulović, S.; Grgurić-Šipka, S. Strong in Vitro Cytotoxic Potential of New Ruthenium-Cymene Complexes. *Organometallics* **2015**, *34*, 3464−3473.
(23) Morgan, A. R.; Pulleyblank, D. E. Native and denatured DNA, cross-linked and pallindromic and circular covalently-closed DNA analyzed by a sensitive fluorimetric procedure. *Biochem. Biophys. Res. Commun.* **1974**, *61*, 396−403.
(24) Birnboim, H. C.; Jevcak, J. J. Fluorometric method for rapid detection of DNA strand breaks in human white blood cells produced by low doses of radiation. *Cancer Res.* **1981**, *41*, 1889.
(25) Das, S.; Saha, A.; Mandal, P. C. Radiation-induced double strand modification in calf thymus DNA in the presence of 1,2 dihydroxy-9,10 anthraquinone and its Cu(II) complex. *Environ. Health Perspect.* **1997**, *105*, 1459−1462.
(26) Das, S.; Mandal, P. C. Anthracyclines as radiosensitizers: a Cu(II) complex of a simpler analogue modifies DNA in Chinese Hamster V79 cells under low-dose γ radiation. *J. Radioanal. Nucl. Chem.* **2014**, *299*, 1665−1670.
(27) Tripathi, R.; Samadder, T.; Gupta, S.; Surolia, A.; Shaha, C. Anticancer activity of a combination of cisplatin and fisetin in embryonal carcinoma cells and xenograft tumors. *Mol. Cancer Ther.* **2011**, *10*, 255−268.
(28) Dasari, S.; Bernard Tchounwou, P. Cisplatin in cancer therapy: molecular mechanisms of action. *Eur. J. Pharmacol.* **2014**, *740*, 364−378.
(29) Gryparis, E. C.; Hatziapostolou, M.; Papadimitriou, E.; Avgoustakis, K. Anticancer activity of cisplatin-loaded PLGA-mPEG nanoparticles on LNCaP prostate cancer cells. *Eur. J. Pharm. Biopharm.* **2007**, *67*, 1−8.
(30) Chen, L.; Li, W.; Wang, H.; Zhao, H.; Tang, J.; Wu, C.; Lu, L.; Liao, W.; Lu, X. Curcumin cytotoxicity is enhanced by PTEN disruption in colorectal cancer cells. *World J. Gastroenterol.* **2013**, *19*, 6814−6824.
(31) Rodriguez, E.; Azevedo, R.; Fernandes, P.; Santos, C. a. Cr(VI) Induces DNA Damage, Cell Cycle Arrest and Polyploidization: A Flow Cytometric and Comet Assay Study in Pisum sativum. *Chem. Res. Toxicol.* **2011**, *24*, 1040−1047.
(32) Stang, A.; Witte, I. Performance of the comet assay in a high-throughput version. *Mutat. Res., Genet. Toxicol. Environ. Mutagen.* **2009**, *675*, 5−10.
(33) Dougan, S. J.; Habtemariam, A.; McHale, S. E.; Parsons, S.; Sadler, P. J. Catalytic organometallic anticancer complexes. *Proc. Natl. Acad. Sci. U.S.A.* **2008**, *105*, 11628−11633.
(34) Molter, A.; Kathrein, S.; Kircher, B.; Mohr, F. Anti-tumour active gold(I), palladium(II) and ruthenium(III) complexes with thio- and selenoureato ligands: a comparative study. *Dalton Trans.* **2018**, *47*, 5055−5064.
(35) Seršen, S.; Kljun, J.; Kryeziu, K.; Panchuk, R.; Alte, B.; Körner, W.; Heffeter, P.; Berger, W.; Turel, I. Structure-Related Mode-of-Action Differences of Anticancer Organoruthenium Complexes with β-Diketonates. *J. Med. Chem.* **2015**, *58*, 3984.
(36) Tian, Z.; Li, J.; Zhang, S.; Xu, Z.; Yang, Y.; Kong, D.; Zhang, H.; Ge, X.; Zhang, J.; Liu, Z. Lysosome-Targeted Chemotherapeutics: Half-Sandwich Ruthenium(II) Complexes That Are Selectively Toxic to Cancer Cells. *Inorg. Chem.* **2018**, *57*, 10498−10502.
(37) Ginzinger, W.; Mühlgassner, G.; Arion, V. B.; Jakupec, M. A.; Roller, A.; Galanski, M.; Reithofer, M.; Berger, W.; Keppler, B. K. A SAR Study of Novel Antiproliferative Ruthenium and Osmium Complexes with Quinoxalinone Ligands in Human Cancer Cell Lines. *J. Med. Chem.* **2012**, *55*, 3398−3413.

https://doi.org/10.1021/acsomega.0c06265
ACS Omega 2021, 6, 8226−8238